Supporting Information

Proposition of Deposition and Bias Conditions for Optimal Signal-to-Noise-Ratio in Resistor- and FET-type Gas Sensors

Wonjun Shin‡, Gyuweon Jung‡, Seongbin Hong, Yujeong Jeong, Jinwoo Park, Donghee Kim, Dongkyu Jang, Dongseok Kwon, Jong-Ho Bae**, Byung-Gook Park, and Jong-Ho Lee*

Department of Electrical and Computer Engineering and Inter-university Semiconductor Research Center, Seoul National University, Seoul 08826, Republic of Korea

**Department of Electrical Engineering and Computer Sciences, University of California at Berkeley, Berkeley, CA 94720 USA.

*E-mail address: ljh@snu.ac.kr

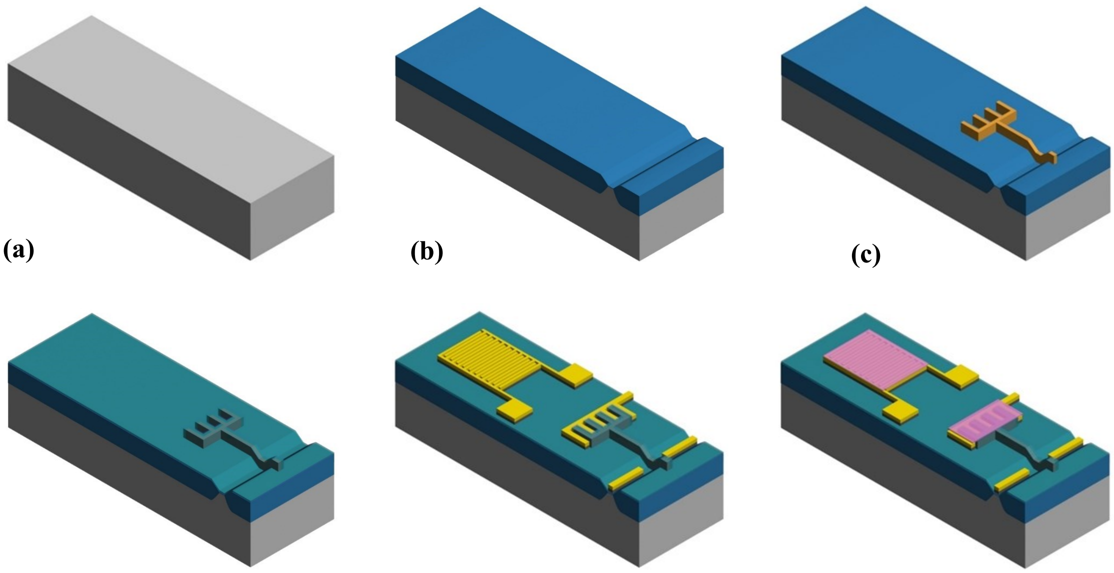

(a) (b) (c) (d) (e) (f)

Figure S1. Schematic cross-sectional views of key process steps cut along dotted lines A-A' and B-B' in Figure 1a. A nitride layer formed on the SiO_2 layer (pad oxide) grown on *n*-type Si substrate is patterned to define active regions (a). Then a 550 nm thick oxide is grown and the nitride is removed (b). The pad oxide is removed and a sacrificial SiO_2 layer is grown. Then ion implantation for the threshold control is performed and the sacrificial layer is removed. After growing 10 nm thick gate oxide, n^+ polycrystalline Si is deposited to form the FG (equivalently gate electrode for normal FETs) (c). Then SiO_2 (10nm)/Si_3N_4 (20nm)/ SiO_2 (10nm) is formed as a passivation layer (O/N/O) (d). After defining contact holes, Cr (30 nm) and Au (50 nm) layers are consecutively formed as the CG, source, and drain electrodes for the FET-type gas sensors and electrodes for the resistor-type gas sensors (e). Then *n*-type In_2O_3 film for sensing layer is deposited (f).

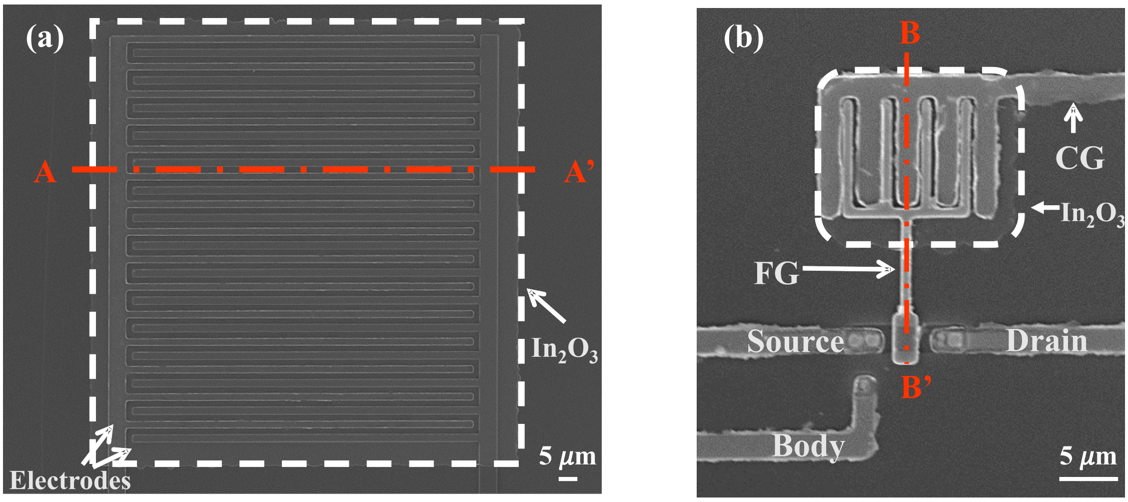

Figure S2. Top SEM images of the fabricated (a) resistor- and (b) FET-type gas sensors. The size of the resistor-type gas sensor is 100×125 μm^2 and the distance between the metal electrodes is 2 μm. The FET-type gas sensor has a FG and a CG facing each other in a horizontal direction. The Width/Length of the FET channel is 2 μm/2 μm and the distance between CG and FG is 0.5 μm. The length (L_f) and number (N_f) of FG fingers are 10 μm and 4, respectively.

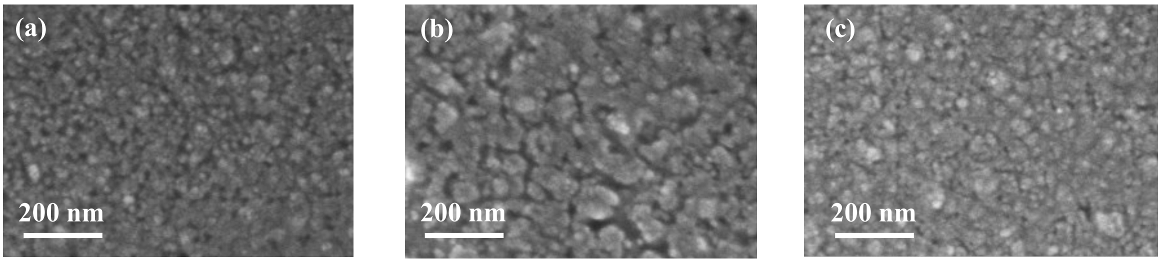

Figure S3. Top SEM images of In_2O_3 films deposited at RF powers of (a) 50 W, (b) 100 W, and (c) 230 W. In_2O_3 film deposited at an RF power of 50 W shows the smallest grain size and In_2O_3 film deposited at an RF power of 100 W shows the largest grain size. The further increase in RF power (230 W) results in a decrease in grain size of In_2O_3 film.

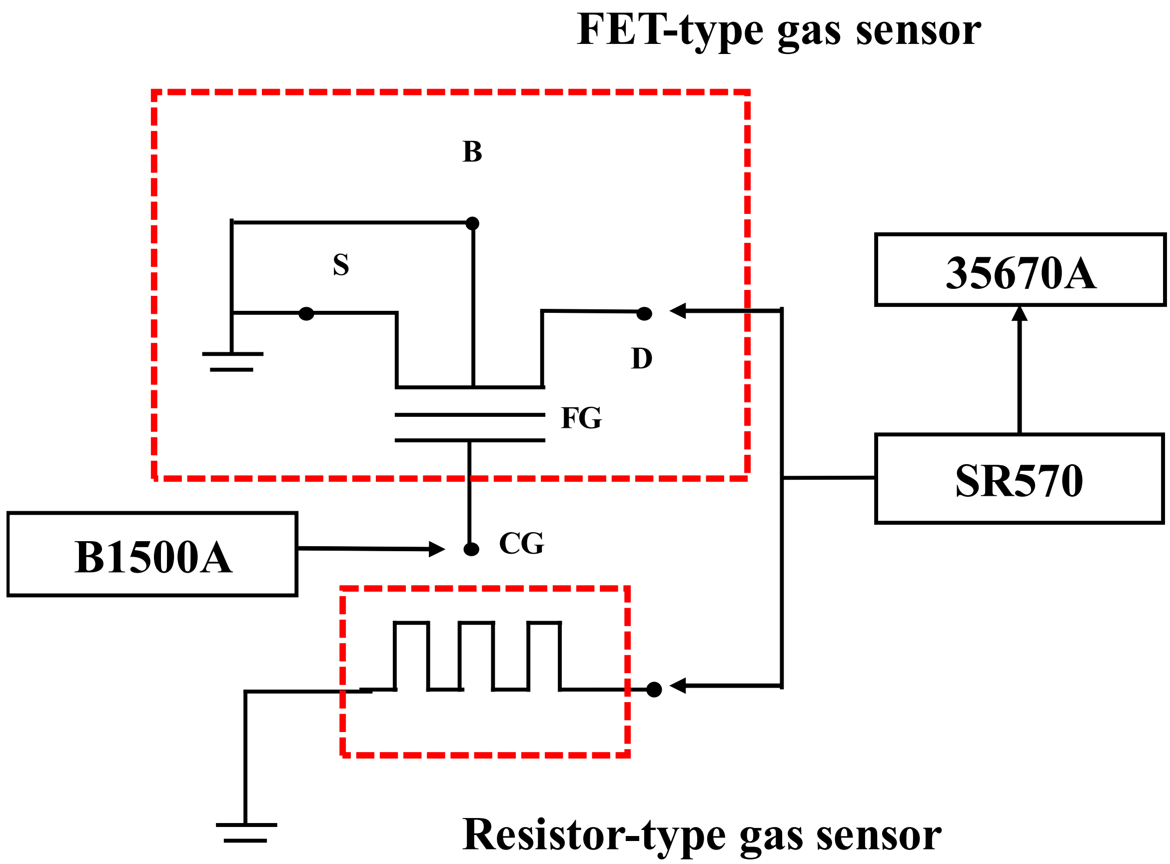

Figure S4. Schematic diagram of the system measuring the gas reaction and the LFN of the sensors. To measure the LFN power spectral density of the sensors, a low noise current amplifier (SR570) and signal analyzer (35670A) are used. The voltage applied to the electrodes (*V*) of the resistor-type gas sensor is supplied by the SR570. The gate voltage and the drain bias of the FET-type gas sensor are supplied by the B1500A and SR570, respectively. The output current of the resistor-type gas sensor or the drain current of the FET-type gas sensor is connected to the SR570 which converts the current fluctuation into a voltage fluctuation. 35670A converts the dynamic signal from SR570 to a power spectral density. The LFN measurement frequency ranges from 10 Hz to 10^4 Hz.

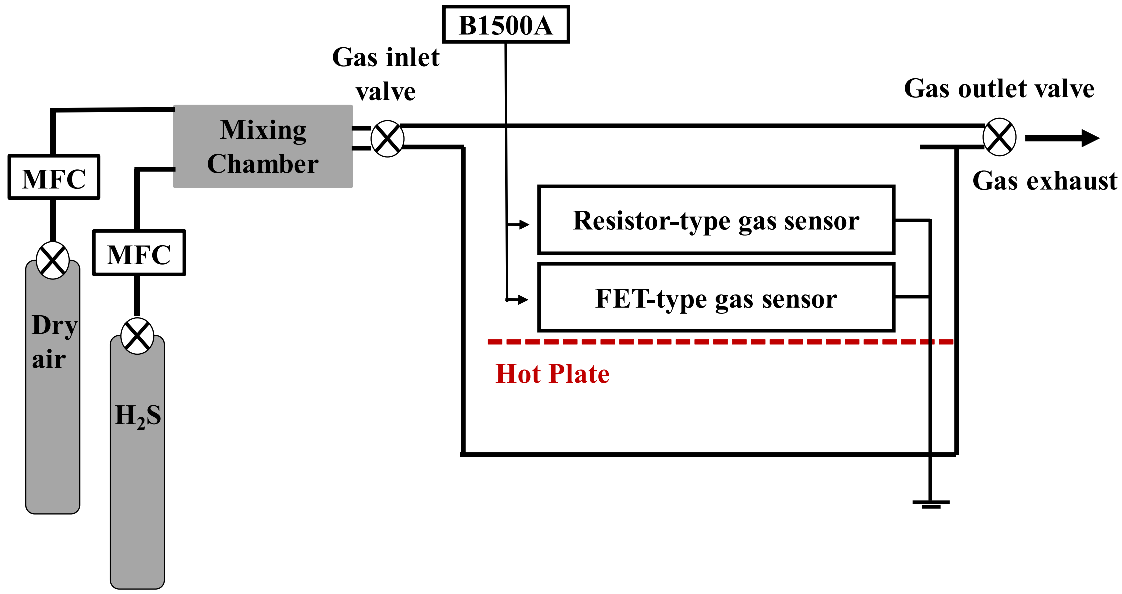

Figure S5. Schematic diagram of the system measuring the gas reaction and the LFN of the sensors. Gas sensing characteristics of the sensors are analyzed by using a semiconductor parameter analyzer (B1500A) and the probe station that contains a test chamber, chuck, gas inlet, and outlet. H_2S gas is used as a target gas and gas flow is controlled by a mass flow controller (MFC). The target gas is mixed with dry air with a relative humidity of 4% for controlling the gas concentration and then the gas is injected into the test chamber. The response of the sensor to the H_2S gas molecules is measured at 180^{o}C.

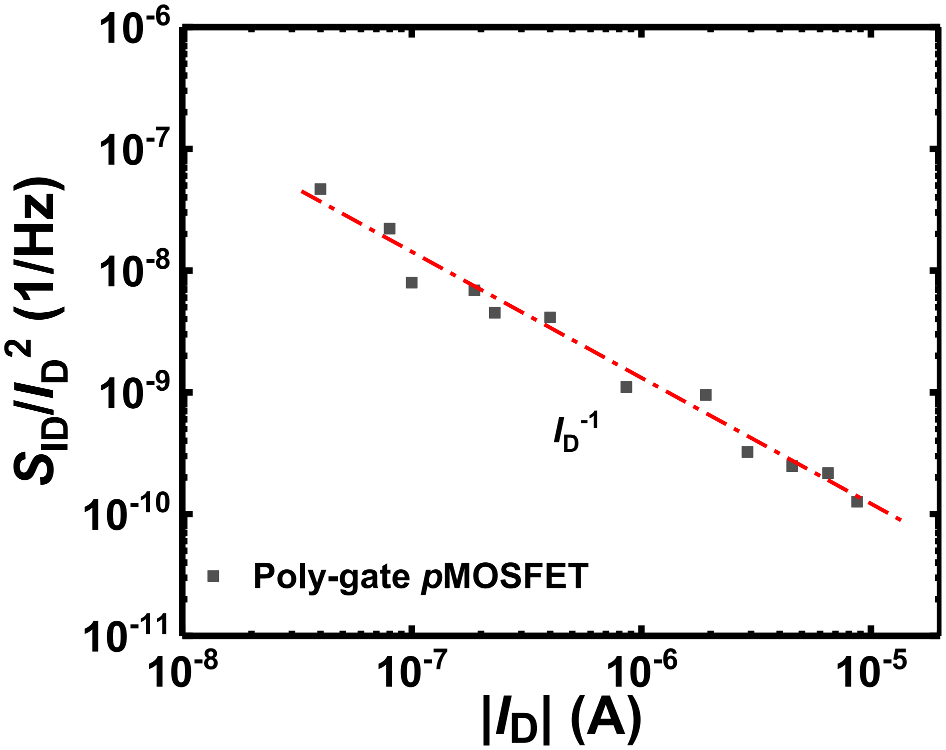

Figure S6. Log-Log plot of S_{ID}/I_D^2 versus I_D of a *p*-type MOSFET with FG as its gate electrode. Dashed dot line represents the fitted LFN characteristics in Figure 3d. The noise characteristics of the *p*-type MOSFET represented in Figure S5 are almost the same as those of the FET type gas sensors represented in Figure 3d. Note that the *p*-type MOSFET and FET-type sensors are fabricated on the same Si substrate and have the same channel size (W/L= 2 μm/2μm). The result demonstrates that sensing material deposition condition does not affect the intrinsic device noise of the FET-type gas sensor. The LFN characteristics of FET-type gas sensors are determined by the *p*-type MOSFET channel noise. It is believed that the additional noise that can be generated at the sensing material has a lower level than the MOSFET channel noise.

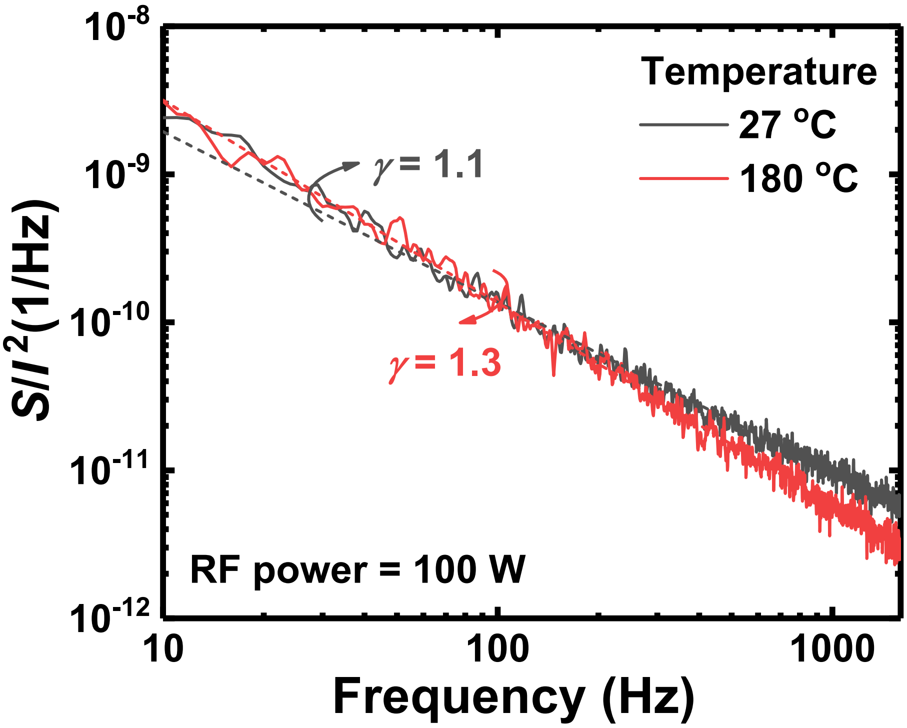

Figure S7. Normalized current noise power spectral density (S_I) of resistor-type gas sensor with In_2O_3 deposited at an RF power of 100 W at 27 ^oC and 180 ^oC. The increase of γ is observed at 180 ^oC.

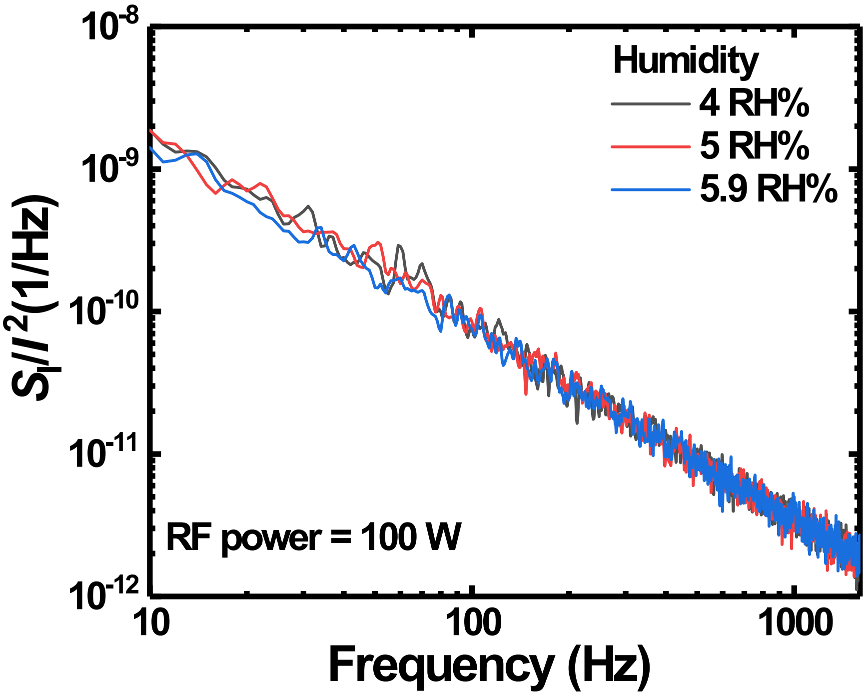

Figure S8. Normalized current noise power spectral density (S_I/I^2) of resistor-type gas sensor with In_2O_3 deposited at an RF power of 100 W with various RH. At 180 °C, pure steam (100°C dew point) will register only ~5.9% on the relative humidity (RH) scale. Figure S7 shows the normalized current noise power spectral density (S_{ID}) of resistor-type gas sensors with In_2O_3 deposited at an RF power of 100 W with various RH. The humidity does not affect the LFN characteristics of the sensor at 180 °C.